
A Generative Framework for Self-Supervised Facial Representation Learning

Ruian He, Zhen Xing, Weimin Tan*, Bo Yan*

School of Computer Science, Shanghai Key Laboratory of Intelligent Information Processing,
Fudan University, Shanghai
{rahe16, xingz20, wmtan, byan}@fudan.edu.cn

Abstract

Self-supervised representation learning has gained increasing attention for strong generalization ability without relying on paired datasets. However, it has not been explored sufficiently for facial representation. Self-supervised facial representation learning remains unsolved due to the coupling of facial identities, expressions, and external factors like pose and light. Prior methods primarily focus on contrastive learning and pixel-level consistency, leading to limited interpretability and sub-optimal performance. In this paper, we propose LatentFace, a novel generative framework for self-supervised facial representations. We suggest that the disentangling problem can be also formulated as generative objectives in space and time, and propose the solution using a 3D-aware latent diffusion model. First, we introduce a 3D-aware autoencoder to encode face images into 3D latent embeddings. Second, we propose a novel representation diffusion model to disentangle 3D latent into facial identity and expression. Consequently, our method achieves state-of-the-art performance in facial expression recognition (FER) and face verification among self-supervised facial representation learning models. Our model achieves a 3.75% advantage in FER accuracy on RAF-DB and 3.35% on AffectNet compared to SOTA methods.

1 Introduction

Human faces hold significant importance in the field of computer vision, serving as carriers of vital information, including identity, expressions, and intentions [16]. Recent advancements in neural networks have led to remarkable achievements in facial understanding [4, 57]. Nonetheless, supervised learning requires large-scale annotated datasets and faces challenges such as imbalance annotation [62, 15] and the labor-intensive labeling work [29]. In response, self-supervised methods [28] has been proposed to tackle this issue by focusing on learning representations rather than directly predicting labels.

General image representation learning methods, such as contrastive learning [7] and masked autoencoders [17], have garnered considerable interest. These models are trained on unlabeled datasets to acquire implicit representations. Nevertheless, the general representations lack interpretability and fail to account for the semantic and structural aspects of the human face.

To leverage the face structure, disentangling is a common practice for learning facial representations. The approach is to distinguish facial expression and identity from changing environments. Prior methods [35, 38, 6, 49] have achieved good results using contrastive learning. However, there are two problems with contrastive facial representation disentangling. First, previous techniques exhibit limitations in terms of spatial awareness and have subpar performance when there is drastic light and pose variations of face images. Second, they focus on pixel-level warping [35, 6], leading to

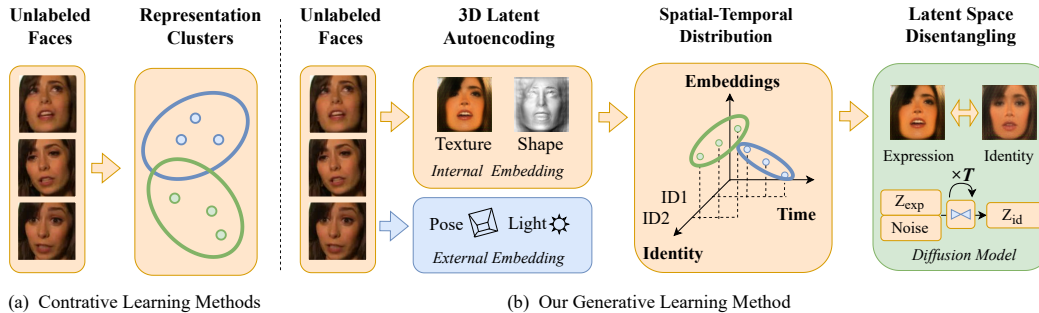


Figure 1: Comparison of different learning paradigm. Our generative framework enables better spatial-temporal awareness and more thorough representation disentangling than previous contrastive learning methods.

the incomplete disentanglement of facial expression. To solve the problems, we suggest that the disentanglement problem can be also formulated as generative objectives in space and time.

Recent advances in generative models, especially those based on diffusion models [20, 51], boost image restoration [25], semantic segmentation [60] and structure prediction [1], which reveal the novel potential of representation learning. Inspired by this, we explore generative approaches in self-supervised facial representation learning. Our contributions to address the problems of previous works are three-fold:

First, we propose LatentFace, a novel generative framework for self-supervised facial representations, as illustrated in Fig. 1. To the best of our knowledge, it is the first 3D-aware latent diffusion model for self-supervised facial representation learning, which has better disentangling ability.

Second, our model incorporates 3D Latent Autoencoding and Latent Space Disentangling. The 3D Latent Autoencoding disentangles the face latent codes in space, while the Latent Space Disentangling predicts the facial identity as the time-invariant part of face latent codes.

Third, extensive experiments have demonstrated that our model achieves state-of-the-art performance on unsupervised facial expression recognition (FER) and face verification. Specifically, our model has a 3.75% advantage in FER accuracy on RAF-DB [33] and 3.35% on AffectNet [40] compared to SOTA unsupervised methods.

2 Methodology

2.1 Revisiting Facial Representation Learning

As illustrated in Fig. 1, our proposed generative framework learns facial expression and identity embeddings from unlabeled images and videos. Given an image I , the facial representation learning models are expected to encode the image as facial embeddings. The facial embedding should be first disentangled from the environment, such as light and facial pose, which can be modeled with a 3D auto-encoding model [59]:

$$\min_{\theta, \phi} \mathbb{E}_I [d(x, D_{\theta}(E_{\phi}(x)))] \quad (1)$$

where I is the image data, D, E are the decoders, and the encoders of pose, light, and facial embeddings. θ and ϕ are the model parameters and d is the distance between the reconstructed image and the original image, usually including photometric loss and perception loss. Next, we consider the discrimination of the facial identity Z_{id} and the facial expression Z_{exp} . In traditional parametrized face models [3], the facial expression is modeled as the deviation of an emotional face from the facial identity. Specifically, the parameters Z_{exp} are for faces of facial expression, and the parameters Z_{id} are for faces with neutral expression, which also refers to facial identity. And the facial expression Δ_{exp} is taken as a bias of neutral face and emotional face:

$$Z_{exp} = Z_{id} + \Delta_{exp} \quad (2)$$

Therefore, the challenge of disentangling facial identity and expression lies in predicting the identity embedding with a given image, which can be learned from the temporal information of videos.

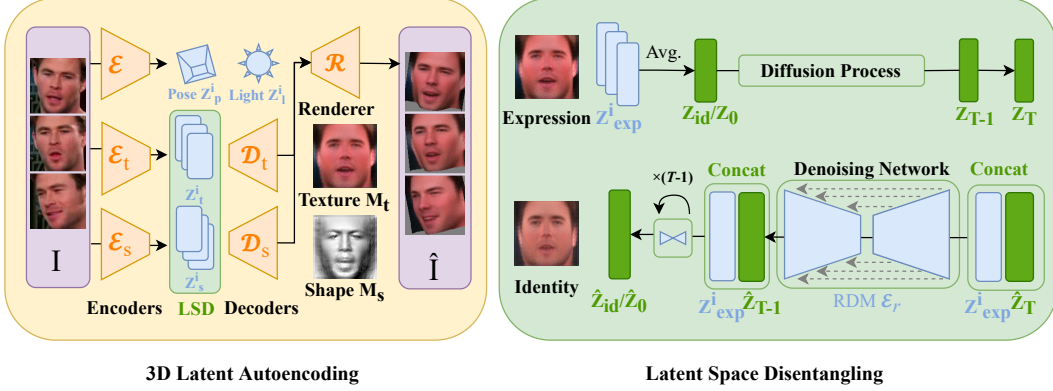


Figure 2: Overview of the proposed framework. In the first stage, we disentangle 3D factors, including texture, shape, pose, and light, through the training of autoencoders (comprising encoders \mathcal{E} and decoders \mathcal{D}) and render them using a renderer \mathcal{R} to reconstruct the input. In the second stage, we further disentangle the texture and shape latent and train the Representation Diffusion Model (RDM) \mathcal{E}_r to generate the identity latent Z_{id} from the emotional face latent Z_{exp} .

We consider the identity embedding Z_{id} should be the same in different frames I_1, I_2 of a video of the same person. Therefore, the optimal embedding Z_{id}^* should meet the following formula.

$$Z_{id}^* = \underset{Z_{id}}{\operatorname{argmax}} p(Z_{id} | I_1, I_2) = \underset{Z_{id}}{\operatorname{argmax}} \left\{ \underbrace{\log p(I_1, I_2 | Z_{id})}_{\text{data term}} + \underbrace{\log p(Z_{id})}_{\text{generation prior}} \right\} \quad (3)$$

where $\log p(I_1, I_2 | Z_{id})$ depends on the construction of input data, while $\log p(Z_{id})$ is the generation prior of Z_{id} . Therefore, how to extract the facial embedding and how to generate Z_{id} becomes the problem. We separately address them with 3D Latent Autoencoding and Latent Space Disentangling.

2.2 3D Latent Autoencoding

As shown in Fig. 2, our framework comprises two stages: 3D latent autoencoding and latent space disentangling. The first stage of our approach is to disentangle 3D facial embeddings, like facial texture Z_t and shape Z_s , from environmental embeddings, including pose Z_p and light Z_l . Leveraging the ample variations in facial and external factors found in image sets [37], the model learns to disentangle them with an autoencoder. We follow Unsup3D [59] to model the face as an unsupervised non-linear parametric model of texture and shape. The facial representations are learned through a self-supervised scheme, which uses the minimal assumption of face symmetry to make the problem converge to stereo reconstruction.

Specifically, the texture and shape of 3D face model are learned by encoders \mathcal{E} and decoder \mathcal{D} with the equation $M = \mathcal{D}(Z) = \mathcal{D}(\mathcal{E}(I))$. In contrast, the light and pose are predicted directly from encoders with the equation $Z = \mathcal{E}(I)$. Finally, the model is trained to reconstruct the input face I by rendering the extracted features and the flipped feature map:

$$\hat{I} = \mathcal{R}(M_t, M_s, Z_p, Z_l), \quad (4)$$

$$\hat{I}' = \mathcal{R}(\operatorname{flip}(M_t), \operatorname{flip}(M_s), Z_p, Z_l), \quad (5)$$

where M_s is the facial shape and M_t is the facial texture. Z_l is the light color and direction, and Z_p is the camera's pose. $\operatorname{flip}(\cdot)$ is a horizontal flip operator. \hat{I} is the reconstructed face, and \hat{I}' is the symmetric face generated from the flipped feature map. For the renderer \mathcal{R} , we implement a differentiable rendering pipeline with a diffuse illumination model and a weak perspective camera using Pytorch3D [24]. We provide detailed implementation in the supplementary materials.

2.3 Latent Space Disentangling

Beyond autoencoding for 3D factors, we further train the model to disentangle facial expressions and identity. While previous work [35, 6] models the facial expression as the pixel-level warping, we propose to predict the time-invariant mean in the latent space, as depicted in Fig. 1.

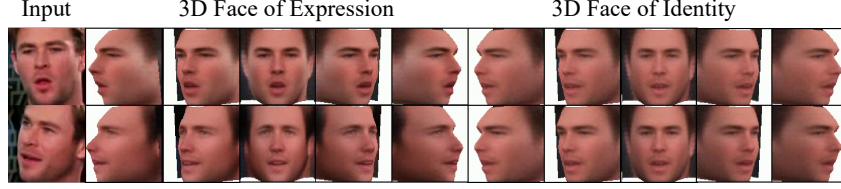


Figure 3: Visualization of generated facial identity. We show the reconstructed 3D face of 2 frames in the input video sequence. The facial identity is disentangled from expressions.

In the second stage, we propose to leverage unlabeled video sequences to construct the learnable data term $\log p(I_1, I_2 | Z_{id})$. Notably, we observe that the web face videos [42] often feature individuals of the same identity with varying facial expressions. Following the neutral face assumption [3], we approximate the identity Z_{id} with the average latent embedding of Z_{exp} in a video sequence, which can be taken as a time-invariant part of the facial attribute.

Specifically, to take texture embedding Z_t as an example, we suppose the autoencoder (\mathcal{E}_t and \mathcal{D}_t) has learned a complete representation of facial texture in the image set. And for every frame $I_i, i = 1, \dots, n$ and n is the number of sampled frames, we can get the encoded embedding Z_t^i for a compressed representation of facial texture. We collect the frames sparsely in a video so that the expression changes significantly to discriminate, and suppose the distribution of \overline{Z}_t can approximate that of Z_{id} . Given the encoded embedding Z_t^i from a video sequence, we denote the embedding Z_t^i as the emotional face embedding Z_{exp} and the average embedding \overline{Z}_t of the sampled sequence as the target facial identity Z_{id} .

2.4 Representation Diffusion Model

Inspired by recent success of latent diffusion models [45], we propose a Representation Diffusion Model (RDM) to generate the facial identity latent with the facial shape and texture latent as the condition. Fig. 2 shows the pipeline of RDM.

For the diffusion process, we sample a noisy embedding Z_τ at time step τ from the identity embedding $Z_0 = Z_{id}$ as:

$$Z_\tau = \sqrt{\bar{\alpha}_\tau} Z_0 + \sqrt{1 - \bar{\alpha}_\tau} \epsilon, \quad \epsilon \sim \mathcal{N}(0, 1) \quad (6)$$

where τ is the diffusion step we use, $\alpha_1, \dots, \alpha_T$ is a predefined noise schedule and $\bar{\alpha}_\tau = \prod_{k=1}^{\tau} \alpha_k$ as defined in [21]. ϵ is the artificial noise sample from a Gaussian distribution $\mathcal{N}(0, 1)$. As the training examples, we randomly add noise to the latent to a diffusion step τ ranging from 1 to $T = 1000$, *i.e.*, $\tau \sim \text{Uniform}(1, T)$.

In the training time, a denoising network \mathcal{E}_r is trained to remove the artificial noise ϵ with the original latent Z_{exp} as the condition. We concatenate the Z_{exp} with the noisy latent Z_t and feed them into \mathcal{E}_r to predict the clean latent $\hat{Z}_0 = \mathcal{E}_r(Z_\tau, \tau, Z_{exp})$. The optimization objective of the UNet can be expressed as follows:

$$\min_{\theta} \mathbb{E}_{Z_0, \epsilon \sim \mathcal{N}(0, 1), \tau \sim \text{Uniform}(1, T)} \|Z_0 - \mathcal{E}_r(Z_\tau, \tau, Z_{exp})\|^2, \quad (7)$$

where Z_{exp} is the embedding of the emotional face and Z_τ is a noisy sample of Z_0 at timestep τ . θ is the parameters of \mathcal{E}_r . RDM is also trained for facial shape embedding Z_s . In the inference time, we use the DDIM [52] sampler at $S = 5$ steps for generating the identity latent \hat{Z}_0 from a random noise $\hat{z}_T \sim \mathcal{N}(0, 1)$. Then we can get the disentangled expression latent Δ_{exp} by subtracting \hat{Z}_0 from Z_{exp} .

3 Experiments

3.1 Implementation Details

Architecture Our proposed model is implemented based on the PyTorch framework. The encoders and decoders are standard fully-convoluted networks with batch normalization layers. The embedding

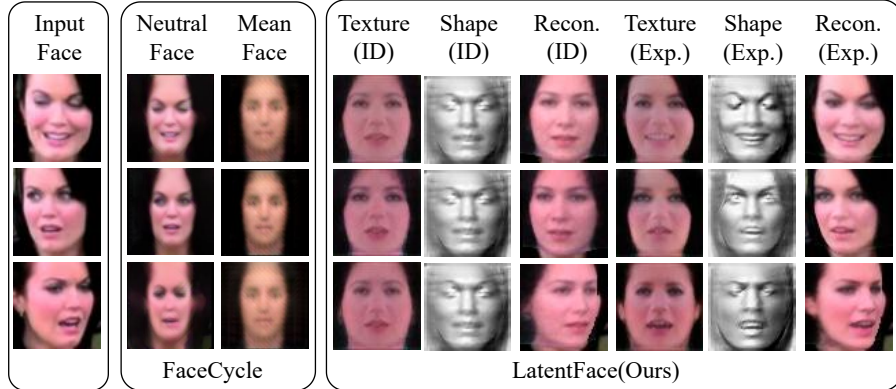


Figure 4: Comparison of disentangled representations. Our method have a more detailed and fidelity representation than the SOTA method FaceCycle [6].

size of Z_s and Z_t are set as 256. The denoising UNet [46] is designed as 3 blocks with two ResNet [19] layers in each block. Detailed network implementation and loss functions can be found in the supplementary material. Training and inferencing codes are also provided.

Training Datasets Our model is trained on CelebA [37] dataset for the first stage and Voxceleb [42] for the second stage. CelebA has 10,177 identities and 202,599 face images. We follow the official split to use 162,257 images for training. VoxCeleb has in total 153,516 video clips of 1,251 speakers. We select 1147 speakers as the training set following this work [41]. We crop the images in CelebA and Voxceleb datasets with MTCNN [48] and resize them to 64×64 .

Training Procedure The model is trained with the Adam optimizer [27]. The model is trained for 30 epochs, in the first stage and the second stage respectively. We set the batch size to 16, and the learning rate is 0.0001 for both training stages. In the second stage, we randomly sample 16 frames in a video sequence for training. The experiments are performed on a server with RTX 3090 GPUs.

3.2 Evaluation Settings

Baselines We compare our model with state-of-the-art self-supervised methods, FAb-Net [28], TCAE [35], Temporal [38], FaceCycle [6], SSLFER [49] and PCL [36]. We adopt the officially released models by the authors. Moreover, we also leverage state-of-the-art self-supervised image representation learning methods, the constrative learning method SimCLRv2 [7] and the masked autoencoders [17], as baselines. We use ResNet50 [19] model for SimCLR and ViT-Base [12] model for MAE. The models are trained on CelebA and VoxCeleb dataset separately for 30 epochs at 224×224 resolution. Finally, we compare with the state-of-art unsupervised face model Unsup3D [59] trained on CelebA to show the effectiveness of latent disentanglement.

Evaluation Protocol We adopt a commonly-used linear probing protocol [17] for representation evaluation. The input is first resized to the corresponding resolution of each baseline. We freeze the backbone feature extraction network and train a batch normalization layer followed by a linear layer after the extracted features to reduce the feature dimension and match the output. The linear layer is trained with Adam [27] optimizer and a learning rate of $1e-3$.

3.3 Evaluation of Interpretable Representations

Fig. 4 shows a qualitative comparison of the extracted face representations. The facial identity and expression of the face extracted by FaceCycle [6] are not fully disentangled. In contrast, our method extracts face material and shape representations disentangled from pose and illumination. Furthermore, our model can disentangle facial expressions and identity better. Compared to FaceCycle’s neutral face, our generated texture of facial identity is closer to the neutral state.

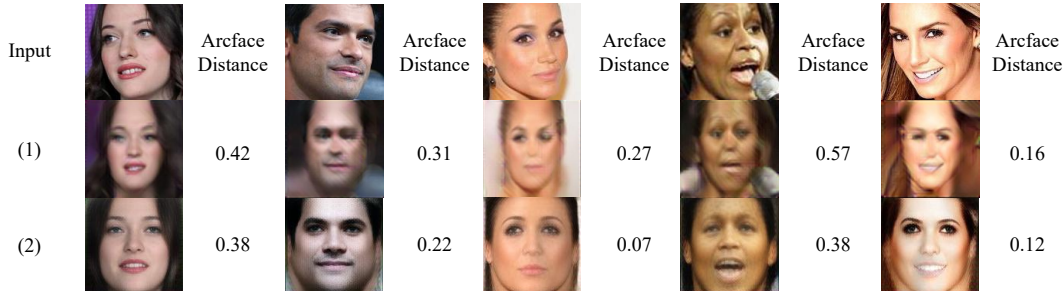


Figure 5: Face frontalization results. (1) is the output of the state-of-the-art method FaceCycle [6]. (2) Our model can restore the complete front face with lower Arcface distance.

Table 1: Facial expression recognition on RAF-DB and AffectNet. Pose 30° and Pose 45° are two subsets of AffectNet with large head poses. We compare the classification accuracy(%)f1-score(%) for all models. Bold text indicates the best results. * means the results are taken from the paper.

Type	Method	RAF-DB		AffectNet		Pose 30°		Pose 45°	
		Acc	F1	Acc	F1	Acc	F1	Acc	F1
Contrastive	SimCLRv2 [7]	64.47	47.48	40.15	38.86	37.69	36.57	37.84	37.41
	FAb-Net [28]	65.54	50.40	36.92	34.83	34.55	33.33	33.18	31.54
	TCAE [35]	69.52	57.90	38.77	37.14	36.56	35.24	35.60	33.67
	Temporal [38]	56.94	42.92	34.20	32.53	34.78	33.47	34.50	32.25
	FaceCycle [6]	71.51	60.80	41.04	39.70	38.50	37.10	36.48	34.90
	SSLFER [49]	55.37	40.37	35.90	34.49	34.72	33.69	34.06	32.15
	PCL* [36]	74.47	-	-	-	-	-	-	-
	PCL [36]	67.07	55.71	36.15	34.74	35.94	34.94	34.72	33.58
Generative	MAE [17]	62.61	48.93	37.40	33.99	35.78	33.05	35.05	32.06
	Unsup3D [59]	69.42	55.50	41.07	39.26	38.89	38.14	36.70	35.25
	Ours	75.26	64.91	44.42	43.60	41.95	41.69	40.43	39.45

Fig. 5 shows the results of face frontalization compared with FaceCycle [6] on the CelebA dataset. With our method, we can synthesize a frontal image of a human face with the extracted facial texture and depth by setting the pose in the canonical view. We compare the cosine distance of Arcface [8] embedding between the frontalized face with the original face. The generated faces of FaceCycle [6] are blurry and have artifacts. Our model can make light and pose disentangled from the environment and restore the color information of the occluded face, which achieves lower Arcface distances.

3.4 Evaluation on Facial Expression Recognition

Facial expression recognition(FER) is a task that divides the expressions on a face image into various categories. We adopt the in-the-wild image facial expression datasets AffectNet [40] and RAF-DB [33, 32]. We adopt seven official facial expressions for RAF-DB and eight for AffectNet. We have cropped the images using provided face boxes for AffectNet and used aligned images for RAF-DB. Because of the unbalanced labels, we follow previous work [31, 61] to downsample the AffectNet dataset. For AffectNet, the test annotation is not released, and we test on the validation set. Our model uses the expression bias Δ_{exp} of texture and shape and the original Z_{exp} for linear probing. And the linear layer is trained for 20 epochs for each dataset.

Tab. 1 reports that our model achieves the best results on the listed datasets, with 75.26% on RAF-DB, and 44.42% on AffectNet. Also, our method has a 3.75% advantage on RAF-DB and 3.35% on AffectNet compared to the state-of-the-art method. Our model achieves state-of-the-art performance compared with other unsupervised methods. We notice that PCL achieves a result far from the original paper, where the linear probing has a long training time of 300 epochs. Furthermore, we follow the paper [57] to test facial pose robustness on two subsets of the AffectNet with head pose at

Table 2: Accuracy(%) comparison on face verification. We show the mean and standard error for the results of 10-fold cross-validation.

Type	Method	LFW	SLLFW
Contrastive	SimCLRv2 [7]	63.38±2.53	54.40±2.45
	FAb-Net [28]	69.57±1.54	56.62±2.13
	TCAE [35]	71.32±1.67	58.05±1.96
	Temporal [38]	65.95±2.89	57.03±3.14
	FaceCycle [6]	71.20±1.90	59.60±2.73
	SSLFER [49]	62.38±2.88	54.55±2.33
	PCL [36]	67.50±2.31	58.12±0.89
Generative	MAE [17]	62.60±2.75	53.05±2.25
	Unsup3D [59]	71.37±1.99	58.70±1.62
	Ours	72.05±2.57	59.72±1.33

Table 3: Ablation study on pixel space disentangling. We show the classification accuracy/f1-score.

Method	RAF-DB	AffectNet
w/o Light	64.21/50.67	33.05/30.43
w/o Pose	67.07/55.02	37.42/35.65
w/o Shape	68.38/58.22	37.67/36.37
w/o Texture	72.58/60.73	41.22/39.24
Full Representations	75.26/64.91	44.42/43.60

30 and 45 degrees separately. Since we disentangle the pose, our model performs excellently, with 41.95% accuracy on 30 degrees and 40.43% on 45 degrees.

3.5 Evaluation on Face Verification

Face verification is the task of comparing a candidate’s face with another face and verifying whether it matches. We use LFW [23, 30] and SLLFW [9, 63] as the test datasets. The datasets have 6000 pairs of face images separately. Different from LFW, SLLFW contains similar-looking face image pairs by human crowdsourcing. We crop images using provided landmarks [56].

We follow the 10-fold cross-validation in the papers [23, 30]. Each image’s facial embedding is extracted first with each model. Then we divide the dataset into ten parts with 300 positive and 300 negative pairs each. We use nine of them to train the linear model and one to test. We repeat this process for cross-validation and report the averaged results in ten folds. Our model uses identity latent Z_{id} of texture and shape and the original Z_{exp} for linear probing.

Tab. 2 shows the evaluation result on the face verification task. Our model disentangles the identity from the expression and considers facial shape and texture separately to get better discrimination. Moreover, the representations are not distracted from expression and external factors, such as light and pose. Therefore, we achieve the best performance among unsupervised methods with an accuracy of 72.05% on LFW and 59.72% on SLLFW.

4 Ablation Study

4.1 3D Latent Autoencoding

We separately remove each 3D face representation from the full model for the ablation study. We remove the shape and texture encoder in the trained model. However, light and pose affect the disentangling of facial shape and texture in the training process. Thus, we remove the light and pose encoders before training. Tab. 3 report the results of facial expression recognition on RAF-DB [33, 32] and AffectNet [40]. The effect of discarding shape and texture latent is 2.68% and 6.88% separately for RAF-DB. The facial shape is more crucial for facial expression recognition. Moreover,

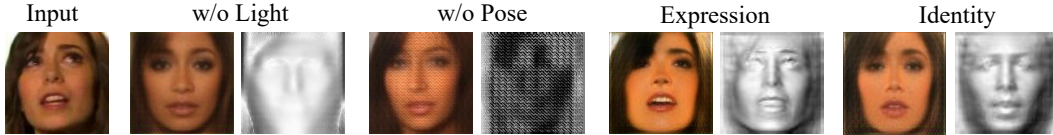


Figure 6: Ablation study of pose, light, expression and identity.

Table 4: Ablation study on latent space disentangling. We show the classification accuracy/f1-score for RAF-DB and AffectNet, and accuracy score for LFW and SLLFW.

Expression	RAF-DB	AffectNet	LFW	SLLFW
None	69.42/55.50	41.07/39.26	71.37±1.99	58.70±1.62
Encoder-based method	73.04/61.37	41.94/40.70	69.00±2.56	57.18±1.27
RDM on Texture	73.98/63.89	42.80/41.82	72.27±2.69	59.37±1.83
RDM on Shape	74.57/64.13	43.47/42.54	71.55±2.31	58.50±1.36
RDM on T & S	75.26/64.91	44.42/43.60	72.05±2.57	59.72±1.33

Fig. 6 shows the effect of removing pose and light. As the light and pose of the face image change greatly, the model converges badly without these two representations.

4.2 Latent Space Disentangling

We also explore an intuitive alternative for latent diffusion. A ResNet [19] encoder can directly predict the facial identity latent. We experiment with the two methods with the same first-stage model. We show the comparison of generated face identity on VoxCeleb [42] dataset test set in Fig. 7. Since the frames are randomly sampled in training, the encoder-based model has a noisy target and generate more artifacts. In contrast, the diffusion-based method is trained to generate from a distribution and has better fidelity.

Tab. 4 compare different latent disentangling methods for the facial expression classification on RAF-DB and AffectNet and facial verification on LFW and SLLFW. The encoder-based method can also disentangle the representation and improve the performance. However, with the diffusion model, the performance boost of latent disentangling is more significant than the encoder-based method, with a 2.24% accuracy advantage on RAF-DB and 2.48% on LFW. Furthermore, we experimented with different diffusion models for different tasks. For facial expression recognition, the disentangling for shape is more important. In contrast, the disentangling for texture has a better improvement on face verification.

5 Related Work

Facial Representation Learning Facial representation learning aims to get better representations of human faces and facilitate downstream tasks, which is usually performed in unsupervised manner. Recent works leverage the image pretraining methods like contrastive learning [5, 18] for an implicit representation from various datasets. FAb-Net [28] learns 2D face motion heat maps from video to learn face representation, while TCAE [35] divides facial movements into action unit (AU)-related and pose-related ones to disentangle facial representations. Lu et al. [38] proposed a model to learn facial features using video contrastive learning algorithms, while FaceCycle [6] progressively disentangle face representations by mining the cyclic consistency of expression and identity. SSLFER [49] and PCL [36] further disentangles facial expressions and poses using a contrastive learning schema. In contrast, our model adopts a generative fashion of representation learning, which is more interpretable and achieve better performance. We also compare the disentangling capability in Tab. 5.

3D Face Modeling 3D face modeling aims to optimize the alignment of face images. One of the most widely used methods is the 3D Morphable Model (3DMM) [3], which models the human face as a linear parameterized 3D model. Many improvements [14, 10, 54, 55, 53] have been made to 3DMM for improved alignment accuracy and natural expression. However, this method requires extensive manual annotation from face scanning, which is expensive and laborious. On the other

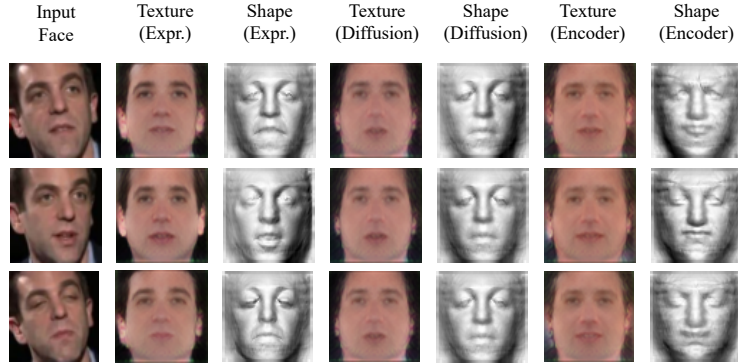


Figure 7: Ablation study of the diffusion model. The encoder-based model have worse ability to generate the identity.

Table 5: Disentangling capabilities comparison. The embedding size is counted for downstream tasks. Our method disentangles more facial factors than previous works while remaining reasonable embedding size.

Method	Identity	Expression	Light	Pose	Texture	Shape	Embedding Size
FAb-Net [28]	✓	✓		✓			256
TCAE [35]		✓		✓			256
Temporal [38]		✓					256
FaceCycle [6]	✓	✓		✓			6272
SSLFER [49]		✓					128
PCL [49]	✓	✓		✓			2048
Unsup3D [59]			✓	✓	✓	✓	512
Ours	✓	✓	✓	✓	✓	✓	1024

hand, unsupervised face models, such as Unsup3D [59] and Lifting Autoencoders [47], have recently gained attention because they do not require face annotations. However, these models have limited design for self-supervised facial representation and has a subpar performance with direct use.

Latent Diffusion Models Diffusion models [20, 51] have emerged as a popular alternative to GANs for image synthesis [11, 43] in the pixel space. These models have also shown successful results in various domains, such as video generation [58, 22], image restoration [25, 39], semantic segmentation [60, 2], and natural language processing [34]. In the diffusion-based framework [20], models are trained on images using score-matching objectives at different noise levels, and sampling is achieved through iterative denoising. [45] have demonstrated the potential of learning the diffusion model in latent space defined by a pretrained autoencoder [13], achieving better quality than ever. Inspired by the success, we explore the use of latent diffusion models for facial representation learning.

6 Conclusion and Discussion of Broader Impact

In this paper, we propose LatentFace, a novel generative framework for self-supervised facial representations. We suggest that the disentangling problem can be also formulated as generation objectives and propose the solution using a 3D-aware latent diffusion model. Experimental results demonstrate that our approach can achieve SOTA performance with high interpretability.

Although our method has achieved superior performance in self-supervised facial representation learning, interpreting a face with a large deflection angle is still not easy due to occlusion. Our model can disentangle the face with up to 60-degree deflection and will support larger angle with proper data. Meanwhile, the extracted representations will reflect the real facial shape and texture, which may be used for further face edition and generation, causing potential application risks. For real application, the decoders can be removed in concerns of privacy.

References

- [1] Josh Abramson, Jonas Adler, Jack Dunger, Richard Evans, Tim Green, Alexander Pritzel, Olaf Ronneberger, Lindsay Willmore, Andrew J Ballard, Joshua Babrick, et al. Accurate structure prediction of biomolecular interactions with alphafold 3. *Nature*, pages 1–3, 2024.
- [2] Dmitry Baranchuk, Ivan Rubachev, Andrey Voynov, Valentin Khrukov, and Artem Babenko. Label-efficient semantic segmentation with diffusion models. *arXiv*, abs/2112.03126, 2021.
- [3] Volker Blanz and Thomas Vetter. A morphable model for the synthesis of 3d faces. In *SIGGRAPH*, page 187–194, 1999.
- [4] Qiong Cao, Li Shen, Weidi Xie, Omkar M. Parkhi, and Andrew Zisserman. Vggface2: A dataset for recognising faces across pose and age. In *FG*, pages 67–74, 2018.
- [5] Mathilde Caron, Ishan Misra, Julien Mairal, Priya Goyal, Piotr Bojanowski, and Armand Joulin. Unsupervised learning of visual features by contrasting cluster assignments. volume 33, pages 9912–9924, 2020.
- [6] Jia-Ren Chang, Yong-Sheng Chen, and Wei-Chen Chiu. Learning facial representations from the cycle-consistency of face. In *ICCV*, pages 9660–9669, 2021.
- [7] Ting Chen, Simon Kornblith, Mohammad Norouzi, and Geoffrey Hinton. A simple framework for contrastive learning of visual representations. In *International conference on machine learning*, pages 1597–1607. PMLR, 2020.
- [8] Jiankang Deng, Jia Guo, Niannan Xue, and Stefanos Zafeiriou. Arcface: Additive angular margin loss for deep face recognition. in 2019 ieee. In *CVPR*, pages 4685–4694, 2018.
- [9] Weihong Deng, Jiani Hu, Nanhai Zhang, Binghui Chen, and Jun Guo. Fine-grained face verification: Fglfw database, baselines, and human-dcmn partnership. *Pattern Recognition*, 66:63–73, 2017.
- [10] Yu Deng, Jiaolong Yang, Sicheng Xu, Dong Chen, Yunde Jia, and Xin Tong. Accurate 3d face reconstruction with weakly-supervised learning: From single image to image set. In *2019 IEEE/CVF Conference on Computer Vision and Pattern Recognition Workshops (CVPRW)*, pages 285–295, 2019.
- [11] Prafulla Dhariwal and Alexander Nichol. Diffusion models beat gans on image synthesis. *NeurIPS*, 34:8780–8794, 2021.
- [12] Alexey Dosovitskiy, Lucas Beyer, Alexander Kolesnikov, Dirk Weissenborn, Xiaohua Zhai, Thomas Unterthiner, Mostafa Dehghani, Matthias Minderer, Georg Heigold, Sylvain Gelly, et al. An image is worth 16x16 words: Transformers for image recognition at scale. *arXiv*, 2020.
- [13] Patrick Esser, Robin Rombach, and Bjorn Ommer. Taming transformers for high-resolution image synthesis. In *CVPR*, pages 12873–12883, 2021.
- [14] Yao Feng, Haiwen Feng, Michael J. Black, and Timo Bolkart. Learning an animatable detailed 3d face model from in-the-wild images. *ACM Trans. Graph.*, 40(4), jul 2021.
- [15] Xiao Gu, Yao Guo, Zeju Li, Jianing Qiu, Qi Dou, Yuxuan Liu, Benny Lo, and Guang-Zhong Yang. Tackling long-tailed category distribution under domain shifts. In *ECCV*, pages 727–743. Springer, 2022.
- [16] Michael E Hasselmo, Edmund T Rolls, and Gordon C Baylis. The role of expression and identity in the face-selective responses of neurons in the temporal visual cortex of the monkey. *Behavioural brain research*, 32(3):203–218, 1989.
- [17] Kaiming He, Xinlei Chen, Saining Xie, Yanghao Li, Piotr Dollár, and Ross Girshick. Masked autoencoders are scalable vision learners. In *CVPR*, pages 16000–16009, 2022.
- [18] Kaiming He, Haoqi Fan, Yuxin Wu, Saining Xie, and Ross Girshick. Momentum contrast for unsupervised visual representation learning. In *CVPR*, pages 9726–9735, 2020.

- [19] Kaiming He, Xiangyu Zhang, Shaoqing Ren, and Jian Sun. Deep residual learning for image recognition. pages 770–778, 2016.
- [20] Jonathan Ho, Ajay Jain, and P. Abbeel. Denoising diffusion probabilistic models. *arXiv*, abs/2006.11239, 2020.
- [21] Jonathan Ho, Ajay Jain, and Pieter Abbeel. Denoising diffusion probabilistic models. In *NeurIPS*, volume 33, pages 6840–6851, 2020.
- [22] Jonathan Ho, Tim Salimans, Alexey Gritsenko, William Chan, Mohammad Norouzi, and David J. Fleet. Video diffusion models. *arXiv*, abs/2204.03458, 2022.
- [23] Gary B. Huang, Manu Ramesh, Tamara Berg, and Erik Learned-Miller. Labeled faces in the wild: A database for studying face recognition in unconstrained environments. Technical Report 07-49, University of Massachusetts, Amherst, October 2007.
- [24] Justin Johnson, Nikhila Ravi, Jeremy Reizenstein, David Novotny, Shubham Tulsiani, Christoph Lassner, and Steve Branson. Accelerating 3d deep learning with pytorch3d. 2020.
- [25] Bahjat Kawar, Michael Elad, Stefano Ermon, and Jiaming Song. Denoising diffusion restoration models. *arXiv*, abs/2201.11793, 2022.
- [26] Alex Kendall and Yarin Gal. What uncertainties do we need in bayesian deep learning for computer vision? In Isabelle Guyon, Ulrike von Luxburg, Samy Bengio, Hanna M. Wallach, Rob Fergus, S. V. N. Vishwanathan, and Roman Garnett, editors, *NeurIPS*, pages 5574–5584, 2017.
- [27] Diederik P Kingma and Jimmy Ba. Adam: A method for stochastic optimization. *arXiv*, 2014.
- [28] A. Sophia Koepke, Olivia Wiles, and Andrew Zisserman. Self-supervised learning of a facial attribute embedding from video. In *BMVC*, page 302, 2018.
- [29] Dimitrios Kollias. Abaw: Valence-arousal estimation, expression recognition, action unit detection & multi-task learning challenges. In *CVPR*, pages 2328–2336, 2022.
- [30] Gary B. Huang Erik Learned-Miller. Labeled faces in the wild: Updates and new reporting procedures. Technical Report UM-CS-2014-003, University of Massachusetts, Amherst, May 2014.
- [31] Hangyu Li, Nannan Wang, Xi Yang, Xiaoyu Wang, and Xinbo Gao. Towards semi-supervised deep facial expression recognition with an adaptive confidence margin. In *CVPR*, pages 4166–4175, 2022.
- [32] Shan Li and Weihong Deng. Reliable crowdsourcing and deep locality-preserving learning for unconstrained facial expression recognition. *TIP*, 28(1):356–370, 2019.
- [33] Shan Li, Weihong Deng, and JunPing Du. Reliable crowdsourcing and deep locality-preserving learning for expression recognition in the wild. In *CVPR*, pages 2584–2593, 2017.
- [34] Xiang Li, John Thickstun, Ishaan Gulrajani, Percy S Liang, and Tatsunori B Hashimoto. Diffusion-lm improves controllable text generation. *NeurIPS*, 35:4328–4343, 2022.
- [35] Yong Li, Jiabei Zeng, Shiguang Shan, and Xilin Chen. Self-supervised representation learning from videos for facial action unit detection. In *CVPR*, pages 10916–10925, 2019.
- [36] Yuanyuan Liu, Wenbin Wang, Yibing Zhan, Shaoze Feng, Kejun Liu, and Zhe Chen. Pose-disentangled contrastive learning for self-supervised facial representation. In *Proceedings of the IEEE/CVF Conference on Computer Vision and Pattern Recognition*, pages 9717–9728, 2023.
- [37] Ziwei Liu, Ping Luo, Xiaogang Wang, and Xiaoou Tang. Deep learning face attributes in the wild. In *ICCV*, pages 3730–3738, 2015.
- [38] Liupei Lu, Leili Tavabi, and Mohammad Soleymani. Self-supervised learning for facial action unit recognition through temporal consistency. In *BMVC*, 2020.

- [39] Ziwei Luo, Fredrik K Gustafsson, Zheng Zhao, Jens Sjölund, and Thomas B Schön. Refusion: Enabling large-size realistic image restoration with latent-space diffusion models. *arXiv*, 2023.
- [40] Ali Mollahosseini, Behzad Hasani, and Mohammad H. Mahoor. Affectnet: A database for facial expression, valence, and arousal computing in the wild. *IEEE Transactions on Affective Computing*, 10(1):18–31, 2019.
- [41] Arsha Nagrani, Samuel Albanie, and Andrew Zisserman. Seeing voices and hearing faces: Cross-modal biometric matching. pages 8427–8436, 2018.
- [42] Arsha Nagrani, Joon Son Chung, and Andrew Zisserman. VoxCeleb: A Large-Scale Speaker Identification Dataset. In *Proc. Interspeech 2017*, pages 2616–2620, 2017.
- [43] Alex Nichol, Prafulla Dhariwal, Aditya Ramesh, Pranav Shyam, Pamela Mishkin, Bob McGrew, Ilya Sutskever, and Mark Chen. Glide: Towards photorealistic image generation and editing with text-guided diffusion models. In *International Conference on Machine Learning*, 2021.
- [44] Bui Tuong Phong. Illumination for computer generated pictures. *Commun. ACM*, 18(6):311–317, jun 1975.
- [45] Robin Rombach, A. Blattmann, Dominik Lorenz, Patrick Esser, and Björn Ommer. High-resolution image synthesis with latent diffusion models. *CVPR*, pages 10674–10685, 2021.
- [46] Olaf Ronneberger, Philipp Fischer, and Thomas Brox. U-net: Convolutional networks for biomedical image segmentation. *arXiv*, abs/1505.04597, 2015.
- [47] Mihir Sahasrabudhe, Zhixin Shu, Edward Bartrum, Rıza Alp Güler, Dimitris Samaras, and Iasonas Kokkinos. Lifting autoencoders: Unsupervised learning of a fully-disentangled 3d morphable model using deep non-rigid structure from motion. pages 4054–4064, 2019.
- [48] Florian Schroff, Dmitry Kalenichenko, and James Philbin. Facenet: A unified embedding for face recognition and clustering. pages 815–823, 2015.
- [49] Yuxuan Shu, Xiao Gu, Guangyao Yang, and Benny P. L. Lo. Revisiting self-supervised contrastive learning for facial expression recognition. In *BMVC*, 2022.
- [50] Karen Simonyan and Andrew Zisserman. Very deep convolutional networks for large-scale image recognition. 2015.
- [51] Jascha Narain Sohl-Dickstein, Eric A. Weiss, Niru Maheswaranathan, and Surya Ganguli. Deep unsupervised learning using nonequilibrium thermodynamics. *arXiv*, abs/1503.03585, 2015.
- [52] Jiaming Song, Chenlin Meng, and Stefano Ermon. Denoising diffusion implicit models. *arXiv*, abs/2010.02502, 2020.
- [53] Ayush Tewari, Florian Bernard, Pablo Garrido, Gaurav Bharaj, Mohamed Elgharib, Hans-Peter Seidel, Patrick Pérez, Michael Zollhöfer, and Christian Theobalt. Fml: Face model learning from videos. In *CVPR*, pages 10804–10814, 2019.
- [54] Ayush Tewari, Michael Zollhöfer, Pablo Garrido, Florian Bernard, Hyeonwoo Kim, Patrick Perez, and Christian Theobalt. Self-supervised multi-level face model learning for monocular reconstruction at over 250 hz. pages 2549–2559, 2018.
- [55] Luan Tran and Xiaoming Liu. On learning 3d face morphable model from in-the-wild images. *TPAMI*, 43(1):157–171, 2021.
- [56] Jun Wang, Yinglu Liu, Yibo Hu, Hailin Shi, and Tao Mei. Facex-zoo: A pytorch toolbox for face recognition. page 3779–3782, 2021.
- [57] Kai Wang, Xiaojiang Peng, Jianfei Yang, Debin Meng, and Yu Qiao. Region attention networks for pose and occlusion robust facial expression recognition. *TIP*, 29:4057–4069, 2020.
- [58] Jay Zhangjie Wu, Yixiao Ge, Xintao Wang, Weixian Lei, Yuchao Gu, Wynne Hsu, Ying Shan, Xiaohu Qie, and Mike Zheng Shou. Tune-a-video: One-shot tuning of image diffusion models for text-to-video generation. *arXiv*, abs/2212.11565, 2022.

- [59] Shangzhe Wu, Christian Rupprecht, and Andrea Vedaldi. Unsupervised learning of probably symmetric deformable 3d objects from images in the wild. *TPAMI*, pages 1–1, 2021.
- [60] Jiarui Xu, Sifei Liu, Arash Vahdat, Wonmin Byeon, Xiaolong Wang, and Shalini De Mello. Open-vocabulary panoptic segmentation with text-to-image diffusion models. *arXiv, abs/2303.04803*, 2023.
- [61] Fanglei Xue, Qiangchang Wang, and Guodong Guo. Transfer: Learning relation-aware facial expression representations with transformers. In *ICCV*, pages 3601–3610, 2021.
- [62] Jiabei Zeng, Shiguang Shan, and Xilin Chen. Facial expression recognition with inconsistently annotated datasets. In *ECCV*, pages 222–237, 2018.
- [63] Nanhai Zhang and Weihong Deng. Fine-grained lfw database. In *2016 International Conference on Biometrics (ICB)*, pages 1–6, 2016.

A Facial Expression Analysis

For facial expression recognition, we further evaluate the confusion matrix of our predictions, as depicted in Fig. 8 and Fig. 9. In AffectNet, the classes with the lowest accuracy are 'disgust' (29%) and 'contempt' (24%). In RAF-DB, the classes with the lowest accuracy are 'surprised' (42%) and fearful (41%). We hypothesize that the classification performance is impacted by the dataset's imbalance. Notably, the 'disgust' and 'contempt' classes in AffectNet comprise the smallest proportion of the dataset, each representing only 5% of the samples in the 'neutral' category. We propose that balancing the downstream dataset might improve classification accuracy.



Figure 8: Confusion matrix analysis on AffectNet dataset. We show actual classes in y-axis and predicted classes in x-axis.

B Network Details

For the architecture of the encoders, we partition them into feature encoders and numerical encoders by structure. The feature encoder refers to the facial texture encoder and the facial shape encoder. They work with the decoder to encode the two-dimensional features of the face. Figure 10 shows the detailed structure. The two encoders have the same architecture, and what they produce is a 256-dimensional vector. We use a fully convolutional architecture to reduce the influence of our features on the position of the pose. Our decoder uses stacked convolutional layers, transposed convolutional layers, and group normalization layers. Figure 12 shows the detailed structure. The network uses a 256-dimensional vector as input. The facial texture decoder produces a 3-channel two-dimensional image output, while the facial shape decoder produces 1 channel. The final texture map and depth map will be scaled by Tanh to the range of -1 to 1.

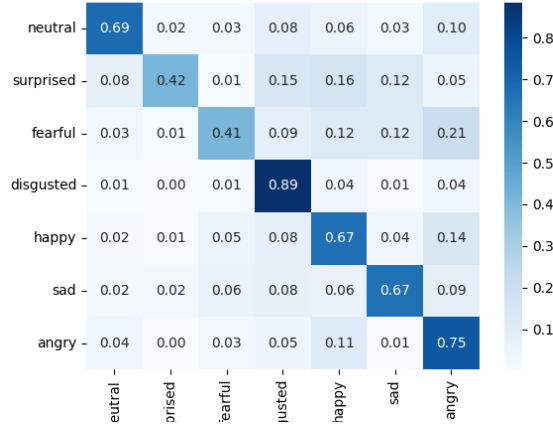


Figure 9: Confusion matrix analysis on RAF-DB dataset. We show actual classes in y-axis and predicted classes in x-axis.

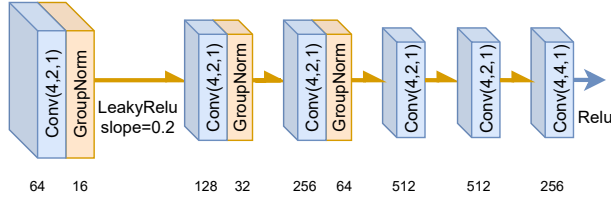


Figure 10: Feature Encoder Architecture. $Conv(a, b, c)$ indicates that the kernel size of the convolutional layer is a , the stride is b , and the padding is c . The number below the convolutional layer indicates the number of convolution kernels. The number below the group normalization layer indicates the number of groups. The yellow arrow indicates Leaky Relu, with a slope of 0.2. And the blue arrow is Relu.

The numerical encoder refers to the light and head pose encoder. Figure 11 shows the detailed structure. They generate corresponding values separately to set the rendering condition. These two encoders have the same structure, except that the output vector dimensions are slightly different. The head pose encoder has 6 dimensions, which are the translation vector of x , y , and z and the rotation angle of yaw, roll, and pitch. The light encoder has 4 dimensions: ambient light parameters, diffuse reflection parameters, and two light directions (x, y) . We will first use Tanh to scale the final outputs to $[-1, 1]$, and then map them to the corresponding space.

Following [59], we use a similar structure as the depth encoders and decoders to generate the confidence map for the self-calibration of the loss function. Figure 14 shows the network structure. We use the $relu3_3$ feature extracted by a pretrained VGG[50] network for feature-level loss. The VGG networks can also be replaced with self-supervised discriminators as demonstrated by [59].

For the architecture of the denoising network, we use one 3 blocks with two ResNet[19] layers in each block. The number of convolution kernels are set to for downsample, middle and upsample. Figure 14 shows the network structure. The input 256-dimensional noise is concatenated with the facial texture latent or the facial shape latent. Therefore, the input size is 512. The output size is 256 dimensional, the same as the input noise. The facial texture latent diffusion model and facial shape latent diffusion model are learned separately.

C Loss Function

In the first stage, our reconstruction loss is composed of a pixel-level loss $L_p(\hat{I}, I)$, a feature-level loss $L_f(\hat{I}, I)$, which measure the photometric discrepancy in pixel level, and feature level separately,

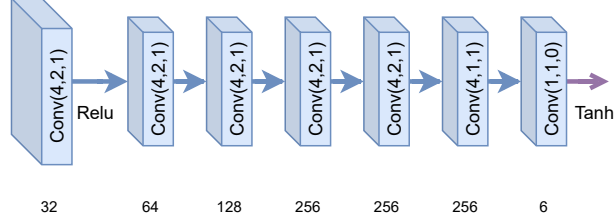


Figure 11: Numerical Encoder Architecture. It is a fully convolutional network. $Conv(a, b, c)$ indicates that the kernel size of the convolutional layer is a , the stride is b , and the padding is c . The number below the module indicates the number of convolution kernels. The blue arrow is ReLU. And the purple arrow is Tanh.

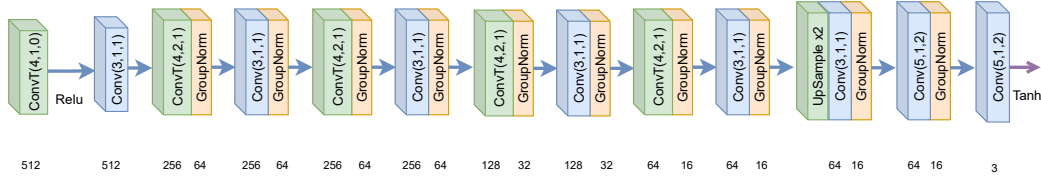


Figure 12: Decoder Architecture. $Conv(a, b, c)/ConvT(a, b, c)$ indicates that the kernel size of the convolutional layer/transposed convolutional layer is a , the stride is b , and the padding is c . The number below the module indicates the number of convolution kernels. And The number below the group normalization layer indicates the number of groups.

which is also used by many works[10, 14, 59].

$$L_p(\hat{I}, I) = L_{conf}(\hat{I}, I, \sigma_p) \quad (8)$$

$$L_f(\hat{I}, I) = L_{conf}(conv(\hat{I}), conv(I), \sigma_f), \quad (9)$$

where I represents the input image and \hat{I} is the reconstructed image. The reconstruction losses are constrained with estimated confidence maps σ to make the model self-calibrate [26].

$$L_{conf}(\hat{I}, I, \sigma) = -\frac{1}{|\Omega|} \sum_{u,v \in \Omega} \ln \frac{1}{\sqrt{2}\sigma_{u,v}} \exp -\frac{\sqrt{2}(\hat{I} - I)_{u,v}}{\sigma_{u,v}} \quad (10)$$

where L is the reconstruction loss, and u, v is the pixel on the rendered face mask Ω . We separately predict the confidence map σ_p and σ_f from the image with an encoder-decoder structure for the pixel-level and feature-level loss. A pretrained VGG[50] is leveraged for the low-level feature extraction network $conv$.

The reconstruction loss $L(\hat{I}, I)$ can be expressed as a linear combination of the pixel-level loss, and the feature-level loss.

$$L(\hat{I}, I) = L_p(\hat{I}, I) + \lambda_f L_f(\hat{I}, I) + \lambda_{flip}(L_p(\hat{I}', I) + \lambda_f L_f(\hat{I}', I)) \quad (11)$$

where λ_f are the weight for the feature-level. Moreover, we also calculate the reconstructed image \hat{I}' of the horizontally flipped shape and texture code for the symmetric loss function. λ_{flip} is the weight for flipped reconstruction loss. The hyperparameters in the loss function are set as follows: $\lambda_f = 1, \lambda_{flip} = 0.5$.

For the second stage, we optimize the denoising U-Net \mathcal{E}_r with Eq. (7). Following [22, 45], we use the SNR weighting strategy, which uses different weights for different steps. For given target latent Z_0 and our predictions \hat{Z}_0 , the denoising loss can be expressed as:

$$L(\hat{Z}_0, Z_0) = E_{Z_0, \epsilon, t} \left[w_t \|Z_0 - \mathcal{E}_r(Z_t, t, Z_{exp})\|^2 \right] \quad (12)$$

where w_t is the SNR weight depended on step t , which can be expressed as $w_t = \frac{\alpha_t^2}{1 - \alpha_t^2}$. α_t is the noise schedule in [20]. Like the latent diffusion models[45], the encoders and decoders are frozen when training the denoising U-Net.

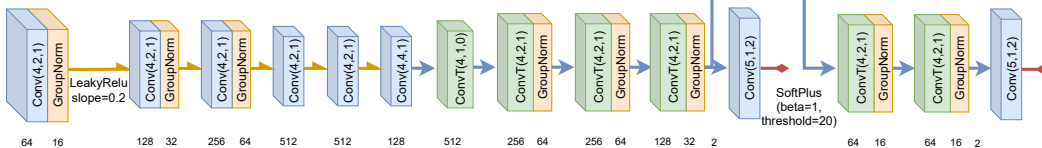


Figure 13: Confidence Map decoder Architecture. The yellow arrow indicates Leaky Relu, with a slope of 0.2. And the blue arrow is Relu. The red arrow is a SoftPlus operator with beta=1 and threshold=20. The shorter path is for the feature level loss and the longer path is for the photometric loss.

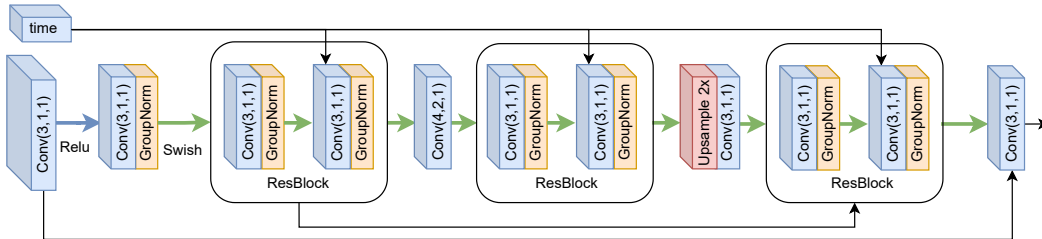


Figure 14: Denoising U-Net Architecture. $Conv(a, b, c)$ indicates that the kernel size of the convolutional layer is a , the stride is b , and the padding is c . The number of convolution kernels are set to 512, 128 and 256. The blue arrow is Relu while the green arrow is Swish Gate. We use sinusoidal timestep embeddings defined in [20]. We omit the skip connections in the ResBlocks[19] for a clear view.

D Rendering Pipeline

In order to render a face image, we need to know: facial shape, facial texture, lighting, and head pose. The facial shape is represented as a two-dimensional single-channel matrix, which represents the depth map of the face. We define a grid, the size of the grid is the same as the image, which is 64×64 . Their x-axis and y-axis coordinates are scaled to between -1 and 1, and then the z-axis coordinates come from the depth map. In this way, we get a three-dimensional model of the human face and the normal of every point for later calculation. The facial texture is represented as a 3-channel 2D matrix in the renderer. It indicates the diffuse reflectance of each face grid point of RGB rays.

Lighting includes ambient light intensity, diffuse reflection intensity and light direction x, y . We are modeling directional light, so only two variables are needed to describe the direction of light. According to the illumination equation [44], we already know the ambient light intensity k_a , diffuse reflection intensity k_d , light direction vector \mathbf{L}_m , and the surface normal vector \mathbf{N}_p of each point, and the diffuse reflection coefficient $k_{d,p}$. Our model ignores the specular reflection of the human face. In most cases, the specular reflection coefficient of the human face is small enough to omit.

The head pose is actually described as the camera parameters. The movement of the head relative to the camera and the change of the camera’s shooting angle are mutual processes. Thus, we only need to control the camera’s shooting displacement vector under x, y, z , and the rotation angle yaw, roll, pitch. We can apply these parameters to the camera imaging equation as below. The displacement vector is \mathbf{t} and the rotation vector is \mathbf{R} . And we define the camera matrix \mathbf{K} as $diag(f, f, 1)$, where f is the focal length. The focal length can be calculated as $\frac{1}{f} = 2 \tan \frac{\theta_{FOV}}{2}$, where θ_{FOV} is set as 10 degrees.

In short, we build a three-dimensional skeleton of the face shape at first, and then map the face material to the three-dimensional skeleton. Then we use the light information to determine the color of the face. Finally, we use the camera formula to get the image we took at a specific angle.